*Proceedings of the*
***Annual Stability Conference***
*Structural Stability Research Council*
*Atlanta, Georgia, April 21–24, 2026*

# Residual stress distribution in cold-formed steel channel section

Alok Kumar Panditaray[1], Bishal Naik[2], Mahendrakumar Mathialagu Madhavan[3], and Gopinath Muvvala[4]

## Abstract

This study investigates residual stress (RS) behavior in Cold-Formed Steel (CFS) unlipped press-braked channel (PBC) sections. A non-destructive X-Ray Diffraction (XRD) technique was used to characterize RS patterns in sections of 1.5 mm and 2.5 mm thickness. Measurements were conducted on specimens post-bending, covering 1116 data points across 54 cross-sections. Results showed peak tensile and compressive residual stresses (TRS and CRS) concentrated at bent locations, while overall RS distributions were irregular and thickness-dependent. To model and predict RS patterns, an Extreme Gradient Boosting (XGBoost) machine learning (ML) model was developed. The model demonstrated high accuracy in capturing the self-equilibrating nature of RS and outperformed other ML models, including Multi-Layer Perceptron (MLP), Decision Tree (DT), and Random Forest (RF) regressors. A finite element (FE) simulation using ABAQUS incorporated the ML-predicted RS to evaluate axial strength in press-braked channel columns. The FE results were validated against the Direct Strength Method (DSM), showing close agreement in both failure modes and load capacity. Stub columns exhibited local buckling, while long columns showed local–flexural interaction, consistent with DSM predictions. A maximum axial strength reduction of 16–17% was observed in 1.5 mm columns due to RS effects, aligned well with existing research. This study emphasizes the critical role of RS in the structural performance of CFS PBC sections and demonstrates the potential of integrating ML-predicted stresses into structural design and assessment.

## 1. Introduction

Cold-formed steel (CFS) is widely used in structural applications due to its high strength-to-weight ratio, corrosion resistance, and fabrication efficiency. Press-braked channel (PBC) sections are commonly employed as load-bearing members; however, the press-braking process introduces significant cold work that affects their structural response. This cold work manifests as residual stresses (RS) and plastic strains associated with strain hardening. While strain hardening increases material strength, residual stresses can adversely influence performance by promoting distortion, buckling, and premature failure (Quach et al. 2010). In press-braked CFS members, residual stresses

[1]Research scholar, Department of Civil Engineering, Indian Institute of Technology Hyderabad,India, <ce23resch01006@iith.ac.in>

[2]Research scholar, Department of Civil Engineering, Indian Institute of Technology Hyderabad,India, <ce20resch11001@iith.ac.in>

[3]Professor, Department of Civil Engineering, Indian Institute of Technology Hyderabad,India, <mkm@ce.iith.ac.in>

[4]Assistant Professor, Department of Mechanical & Aerospace Engineering, Indian Institute of Technology Hyderabad,India, <mgopinath@mae.iith.ac.in>

arise from both coiling–uncoiling and localized cold bending at corner regions (Quach et al. 2009b). Most analytical and design models represent these effects using simplified residual stress distributions and idealized mechanical property variations between flat and corner zones, often based on limited experimental data (Quach et al. 2009a; Quach et al. 2010). Experimental studies indicate that residual stresses reduce stiffness, accelerate plasticity, and decrease fatigue resistance, thereby lowering the load-carrying capacity and stability of thin-walled members (Gardner and Yun 2018.

Previous research has shown that residual stress magnitude and distribution depend strongly on the fabrication method. Roll-formed sections generally develop higher residual stresses due to greater accumulated cold work, whereas press-braked sections exhibit tensile stresses on outer surfaces and compressive stresses on inner surfaces, with notable differences between flat and bent regions (Batista and Rodrigues 1992; Young and Lui 2005. These stresses can reduce CFS column strength by up to 35%, particularly at higher slenderness ratios, with flat-region residual stresses having a more pronounced influence on longer members (Lee and Ketter 1958; Weng and Pekoz 1990; Quach et al. 2010). Conventional residual stress measurement techniques such as sectioning and hole-drilling are destructive and unsuitable for thin-walled CFS sections (Somodi and Kövesdi 2017; Ma et al. 2015). In contrast, X-ray diffraction (XRD) enables accurate, non-destructive quantification of surface residual stresses and is well suited for cold-formed members (Genzel et al. 2012; Wang et al. 2020). Despite its advantages, systematic XRD-based studies on press-braked CFS channel sections remain limited.

This study employs X-ray diffraction to measure residual stress distributions in 1.5 mm and 2.5 mm thick press-braked CFS channel sections. The results provide improved insight into fabrication-induced residual stresses and their implications for structural performance and design.

## 2. Experimental Program

### *2.1 X-ray diffraction measurements*

Residual stresses were measured using an iXRD X-ray stress analyzer (Proto Manufacturing Inc., USA) (PROTO Manufacturing 2016), as shown in Fig. 1(a). A non-destructive X-ray diffraction (XRD) technique compliant with ASTM E915 was employed to quantify residual stresses in cold-formed steel press-braked channel sections (Belassel et al. 2004). The method is based on Bragg's law (Bragg 1912), whereby elastic lattice strains are inferred from variations in interplanar spacing (Jandera and Machacek 2007). The system utilized Cr–K$\alpha$ radiation with a dual-detector configuration to capture lattice spacing variations (Belassel et al. 2004; Celard et al. 2000), as illustrated in Fig. 1(c). Residual stresses were evaluated using the $\sin^2\psi$ method, in which shifts in the diffraction angle (2) at multiple $\psi$ tilts were analyzed to obtain lattice strain from the $\sin^2\psi$ plot and subsequently converted to stresses using Hooke's law (Cooper 1962; Duan et al. 2012). Similar XRD-based procedures have been shown to be effective for characterizing residual stress distributions in press-braked cold-formed steel members (Fig. 1(b)). In the present study, measurements were performed at eleven $\psi$ orientations ranging from $-20°$ to $+20°$, with a defined $\beta$ tilt between the specimen surface and the incident X-ray beam, as illustrated in Fig. 1(d). Longitudinal residual stresses were measured using a 2 mm collimator, an exposure time of 1 s, a $\beta$ oscillation of 3°, a diffraction angle of $2\theta = 156.41°$, and an X-ray wavelength of $\lambda = 2.291$ Å (Suzuki and Shobu 2010).

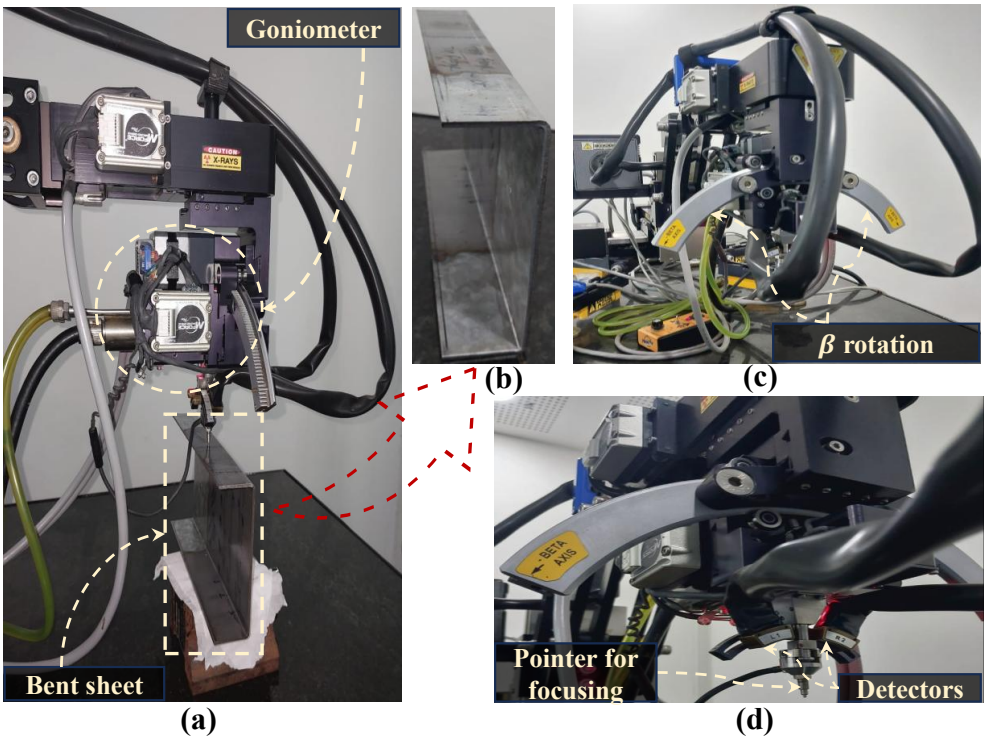


Figure 1: RS measurements setup by XRD : (a) RS measurements on a PBC sheet ; (b) press-braked channel ; (c) $\beta$ rotation of the XRD machine ; (d) pointer and detectors of the XRD machine

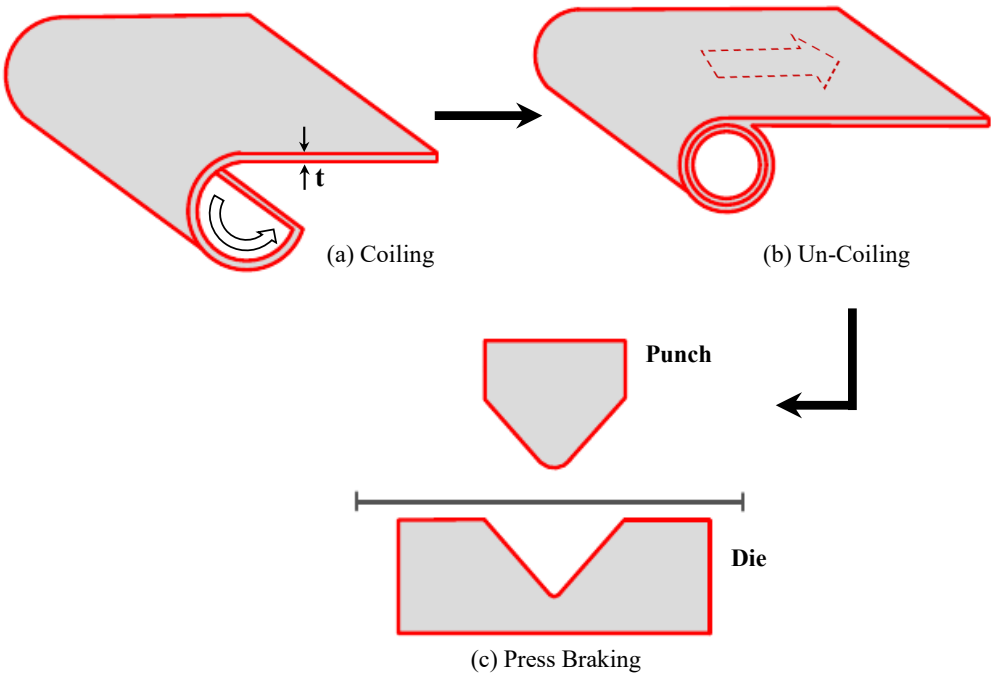


Figure 2: Press-braking fabrication sequence for cold-formed steel sections: (a) coiling; (b) uncoiling and flattening; (c) press braking

### 2.2 Specimen fabrication and material properties

Cold-formed steel (CFS) channel sections used in this study were produced using a press-brake forming process. Press braking offers precise control over bend angles and is well suited for small-batch or custom geometries. Flat sheets (170 mm × 200 mm), cut from galvanized coils, were bent into unlipped channel sections with a flange width of 30 mm, a web width of 110 mm, and a total length of 200 mm. Prior to forming, it was assumed that any residual stresses from rolling were relieved through coil annealing; thus, the residual stresses in finished sections mainly arise from (a) coiling–uncoiling of flat regions and (b) localized cold bending during press braking.The brake press forms the profile through sequential bending along predefined lines using a punch–die assembly. This induces characteristic tensile–compressive stress patterns across the web and flange regions, along with strain hardening at the corners. A schematic of the press-brake system and loading sequence is shown in Fig. 2. To ensure reliability of X-ray diffraction (XRD) measurements, galvanized coatings were removed selectively using hydrochloric acid, followed by surface cleaning and WD-40 application to prevent corrosion. Mechanical properties of the base material were determined through tensile coupon tests conducted in accordance with ASTM E8. Test coupons were extracted using electrical-discharge machining (EDM) and tested in a 30 kN universal testing machine equipped with a 50 mm extensometer. The measured yield strengths were 317.23 MPa for the 1.5 mm thick sheets and 330.26 MPa for the 2.5 mm thick sheets. The corresponding mechanical properties obtained from the stress–strain response are summarized in Table 1.

Table 1: Tensile properties of CFS base metal

| **CFS coupons** | $f_y$ (MPa) | $f_u$ (MPa) | $E_s$ (GPa) | $\epsilon_f$ (%) |
|---|---|---|---|---|
| **1.5 mm thickness** | | | | |
| Coupon 1 | 317.04 | 365.74 | 204.02 | 38.14 |
| Coupon 2 | 310.66 | 359.62 | 201.81 | 35.01 |
| Coupon 3 | 324.00 | 353.09 | 206.81 | 37.08 |
| Mean | 317.23 | 359.48 | 204.21 | – |
| **2.5 mm thickness** | | | | |
| Coupon 1 | 338.00 | 376.07 | 202.35 | 32.09 |
| Coupon 2 | 328.41 | 376.65 | 201.71 | 31.67 |
| Coupon 3 | 324.37 | 369.89 | 200.39 | 32.75 |
| Mean | 330.26 | 374.20 | 201.48 | – |

$*$ $E_s$: Young's modulus of steel $*$ $\epsilon_f$: Strain at fracture

### 2.3 Residual stress measurement configuration

Residual stresses in the press-braked channel specimens were measured using XRD, focusing on the longitudinal stress component. The test program included twelve channels of 1.5 mm thickness and six channels of 2.5 mm thickness. Measurements were taken 77.5 mm from one end—corresponding to the mid-length of the 200 mm specimens—to avoid end effects, as illustrated in Fig. 3(a). Each channel contained three measured cross-sections spaced 22.5 mm apart, denoted as Cross Section

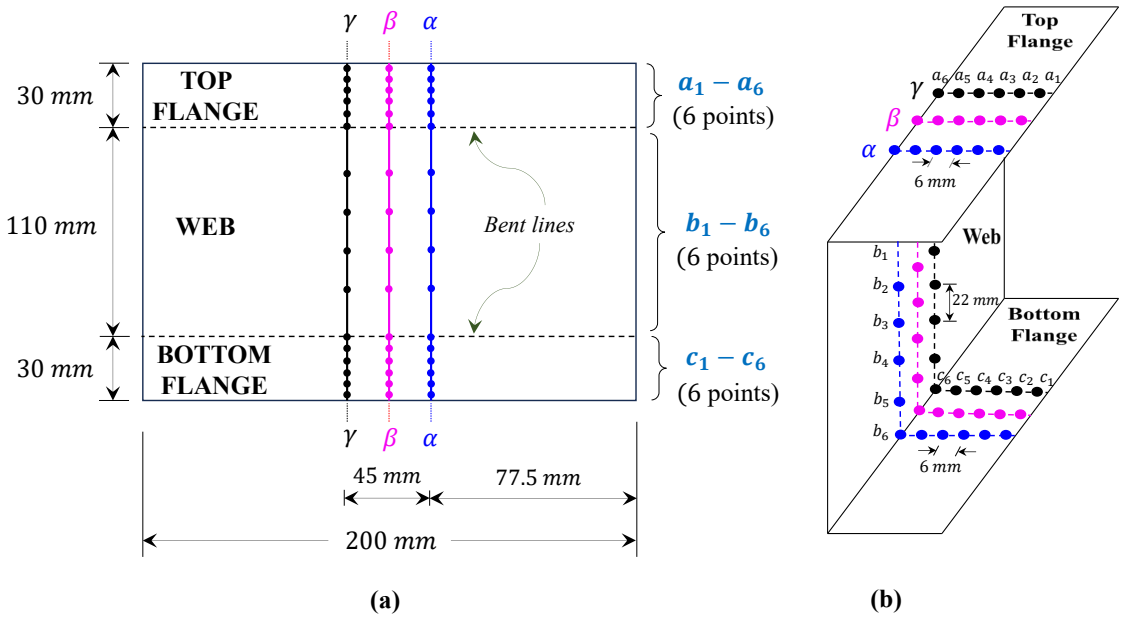


Figure 3: Schematic of residual stress measurement locations on (a) flat sheet and, (b) press-braked channel

1 (CS 1, $\alpha$), Cross Section 2 (CS 2, $\beta$), and Cross Section 3 (CS 3, $\gamma$), as shown in Fig. 3(b). At each section, 22 points were measured: 12 on the flanges (6 outer-top and 6 outer-bottom) and 10 on the web (6 inner and 4 outer), with reduced spacing near the edges to capture stress gradients. For the 1.5 mm channels, six specimens included all web and flange points (396 points), while six excluded outer-web locations (324 points), giving a total of 720 measurements. The 2.5 mm channels added 396 points, resulting in 1116 XRD measurements overall. This arrangement effectively captures the residual stresses induced by coiling–uncoiling and cold bending in press-braked CFS channel sections.

## 3. Results and Discussion

### *3.1 Experimental observations*

Residual stresses in the 1.5 mm and 2.5 mm PBC sections were evaluated using XRD at selected flange and web locations. The 1.5 mm specimens were examined in two configurations: the first measured RS on outer flanges and inner web surfaces, while the second included both inner and outer web surfaces along with the outer flanges. In both cases, RS profiles exhibited substantial scatter, with no consistent trend in the flat regions. Representative RS distributions for a 1.5 mm PBC section are presented in Fig. 4. Similar residual stress patterns were observed across the remaining 1.5 mm and 2.5 mm PBC sections. Across all measurements, a consistent feature was observed at the bent corners: the outer surface exhibited tensile residual stress (TRS), while the inner surface showed compressive residual stress (CRS), reflecting strain reversal during the cold-bending process. The flat portions of the flange and web exhibited mixed tensile–compressive behavior without a clear through-thickness trend, indicating competing influences from coiling–uncoiling and press-braking operations. Irrespective of section thickness, both the 1.5 mm and 2.5 mm PBC sections exhibited similar residual stress characteristics, with tensile stresses on the outer surface and compressive stresses on the inner surface at the bends, and irregular stress variations in the flat regions. This

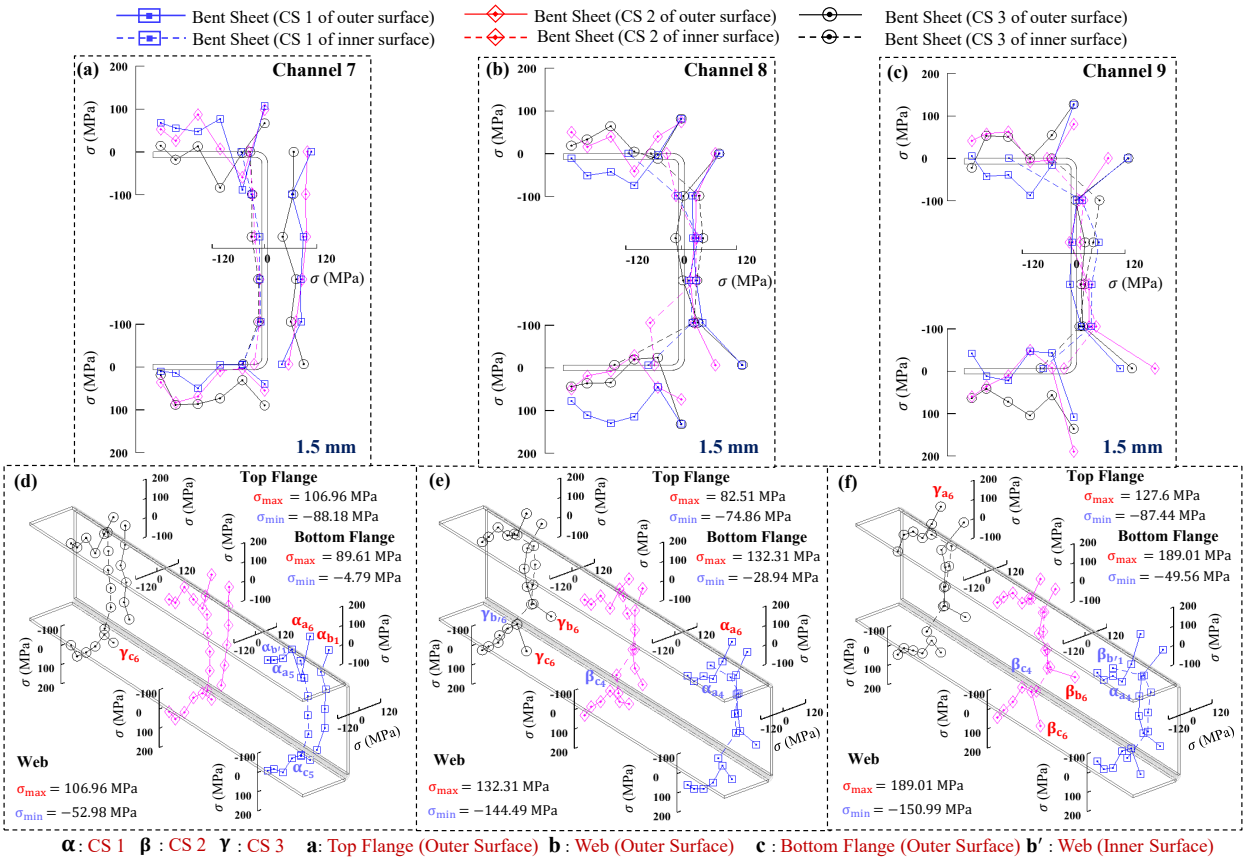


Figure 4: Residual stress distributions in 1.5 mm press-braked CFS channels (7–9): 2D plots are shown in (a–c), with the corresponding 3D plots in (d–f)

consistency across thicknesses suggests that localized plastic deformation at the bent corners, rather than thickness alone, governs the dominant residual stress response (Quach et al. 2010).

### *3.2 Residual stress characteristics in press-braked channel sections*

RS measurements obtained from XRD reveal substantial spatial variability in both 1.5 mm and 2.5 mm press-braked CFS channel sections. Although no uniform RS pattern is observed across flanges or webs, consistent trends emerge at bent locations, which govern the overall stress behavior. For the 1.5 mm sections, the outer surfaces of bent flanges exhibit peak TRS of up to approximately 60% of the yield stress ($f_y$), while the corresponding inner surfaces develop CRS approaching 48% of $f_y$. In flat flange regions, TRS ranges from 23–53% of $f_y$ and CRS from 18–43% of $f_y$. Web stresses are comparatively lower, with TRS between 1–30% and CRS between 4–29% of $f_y$. Residual stress differences are more pronounced in the flanges (44–81% of $f_y$) than in the web, particularly on the inner web surface, indicating stronger through-thickness variability. In the 2.5 mm sections, similar behavior is observed. Peak TRS at bent flange locations ranges from 10–65% of $f_y$, while CRS at the corresponding inner surfaces reaches up to 41% of $f_y$. Flat flange regions show TRS of 17–41% and CRS of 6–44% of $f_y$, whereas web stresses range from 4–33% (TRS) and 1–18% (CRS). Residual stress variation in the flanges (25–84% of $f_y$) remains higher than in the web, where inner and outer surfaces exhibit comparable ranges. A comparison of both

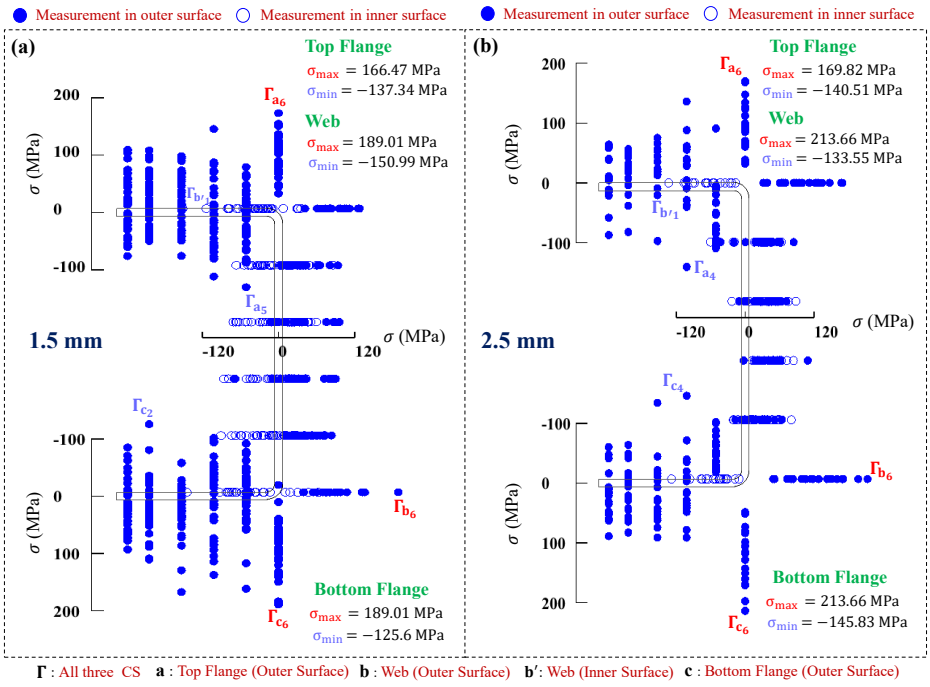


Figure 5: Two-dimensional scatter plots of measured residual stresses in press-braked channel sections: (a) 1.5 mm thickness; (b) 2.5 mm thickness

thicknesses, as illustrated in Fig. 5, confirms that bent corners are the most critical RS zones, consistently showing tensile stresses on the outer surface and compressive stresses on the inner surface due to strain reversal during cold bending. Flat regions of both flanges and webs display considerable scatter with no dominant trend. The 1.5 mm webs exhibit greater inner–outer stress variability than the 2.5 mm webs, indicating a more pronounced through-thickness gradient. In the flanges, both thicknesses show nearly balanced TRS and CRS in the top flange, whereas the bottom flange is tensile-dominant in the 1.5 mm sections and comparatively more compressive in the 2.5 mm sections.

Overall, while thickness influences the magnitude and variability of residual stresses—particularly in the web—the fundamental RS distribution pattern remains similar. The formation of tensile–compressive stress pairs at bent locations is primarily governed by bending severity and localized plastic deformation rather than thickness alone.

### *3.3 Residual stress prediction using machine learning*

The pronounced variability in experimentally measured RS, particularly between 1.5 mm and 2.5 mm press-braked channel sections, motivates the use of machine learning (ML) to capture complex, non-uniform stress patterns. A comprehensive dataset comprising 1116 XRD-based RS measurements was assembled from press-braked CFS channel specimens, covering both thicknesses, multiple cross-sections, and distinct geometric regions including flanges, web, and bent corners.Four supervised ML regression models—Decision Tree (DT), Random Forest (RF), Multi-Layer Perceptron (MLP), and Extreme Gradient Boosting (XGBoost)—were implemented and compared. Input features included cross-section index, spatial coordinates, measurement location

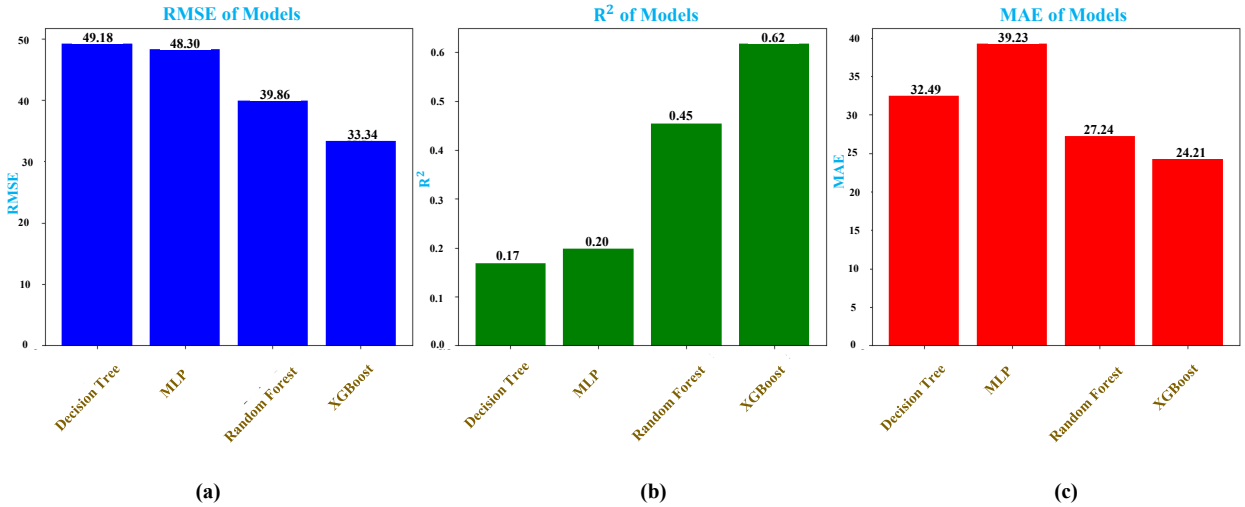


Figure 6: Comparison of predictive performance of machine learning models based on evaluation metrics: (a) RMSE ; (b) $R^2$ ; (c) MAE

(flange or web), surface type (inner or outer), and sheet thickness. The dataset was randomly divided into training (80%) and testing (20%) subsets to ensure unbiased evaluation. Model performance was assessed using the coefficient of determination ($R^2$), mean absolute error (MAE), and root mean square error (RMSE). Among the evaluated models, XGBoost consistently provided the most accurate predictions as shown in Fig. 6, demonstrating superior generalization capability across both thicknesses.

### *3.4 XGBoost model optimization and performance*

To further enhance prediction accuracy, the XGBoost model was optimized through systematic hyperparameter tuning using GridSearchCV, RandomizedSearchCV, and Optuna frameworks. These approaches explored a wide parameter space to improve predictive accuracy while maintaining physical consistency of the RS field. In addition to standard error metrics, the predicted stress distributions were post-processed to compute resultant residual forces across flanges and web surfaces, ensuring near self-equilibrium of stresses.Net residual forces were calculated using a combination of numerical integration schemes, including Simpson's rule for uniformly spaced data, the trapezoidal rule near boundaries, and linear interpolation through bent regions. Model robustness was verified using three-fold cross-validation to mitigate overfitting. The optimized XGBoost model achieved the highest $R^2$ values and the lowest MAE and RMSE for both 1.5 mm and 2.5 mm sections, with consistent performance on training and test datasets, as shown in Fig. 7. These results indicate that the XGBoost model provides accurate residual stress predictions with stable performance across training and test datasets, suggesting no overfitting and supporting its use for further numerical and design-based investigations.

The ensemble XGBoost model successfully predicts residual stress distributions in press-braked CFS channel sections for both 1.5 mm and 2.5 mm thicknesses, as shown in Fig. 8. The model captures RS on the inner and outer web surfaces, bent regions, and outer flange surfaces, including the otherwise difficult-to-measure inner flange surfaces. For the 1.5 mm sections, distinct RS profiles are observed between inner and outer surfaces across the cross-section. In contrast, for

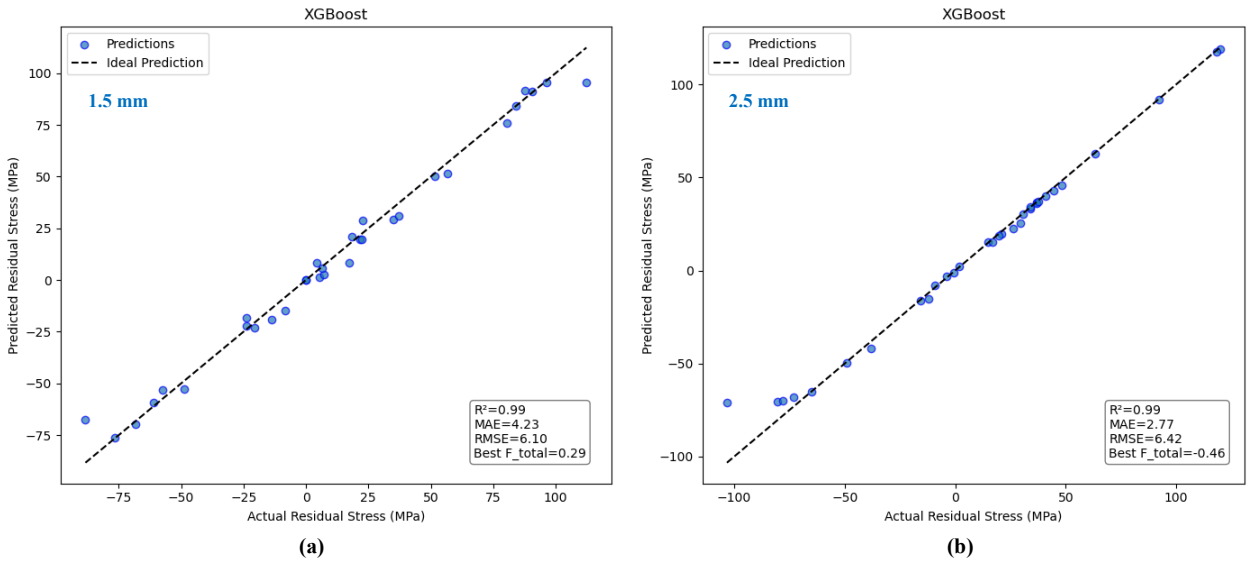


Figure 7: Performance comparison of ensemble XGBoost ML model: (a) 1.5 mm PBC ; (b) 2.5 mm PBC

the 2.5 mm sections, this distinction is reduced in flat regions, with inner and outer RS values becoming comparable, except at bent locations where clear tensile–compressive pairs persist. In both thicknesses, the predicted RS distributions satisfy self-equilibrium, confirming the physical consistency of the ML predictions. Maximum RS values are consistently observed at bent locations due to cold bending. For the 1.5 mm section, the maximum TRS occurs at the outer surface of the bottom flange bend, reaching 30.36% of $f_y$, while the corresponding CRS at the inner surface reaches 28.21% of $f_y$. For the 2.5 mm section, higher magnitudes are predicted, with maximum TRS and CRS of 36.18% and 30.82% of $f_y$, respectively. These results confirm that bending-induced plastic deformation governs RS concentration, with higher thickness leading to increased stress magnitudes. Overall, the XGBoost model demonstrates high predictive accuracy without evidence of overfitting, providing reliable, self-equilibrated RS fields suitable for subsequent numerical simulations and design-oriented analyses. A preliminary finite element study incorporating the ML-predicted RS is therefore conducted in the following section to evaluate axial strength behavior of press-braked channel columns.

### *3.5 Numerical evaluation of ML-predicted residual stresses*

Finite element (FE) analyses were performed using ABAQUS (Hibbitt, Karlsson and Sorensen, Inc. 2002) to quantify the influence of machine-learning (ML)–predicted residual stresses (RS) on the axial compression behavior of press-braked unlipped CFS channel columns with thicknesses of 1.5 mm and 2.5 mm. The columns shared identical geometry and material properties (Table 1, Fig. 3) and were modeled with fixed-end boundary conditions. Nonlinear material behavior, geometric imperfections, and ML-predicted RS were incorporated to capture realistic structural response.The true stress $\sigma_{\text{true}}$ and plastic true strain $\varepsilon^{\text{pl}}_{\text{true}}$ were calculated using Eqs. 1 and 2 (Ellobody and Young 2005) and used for numerical modeling in this study.

$$\sigma_{\text{true}} = \sigma(1+\varepsilon) \tag{1}$$

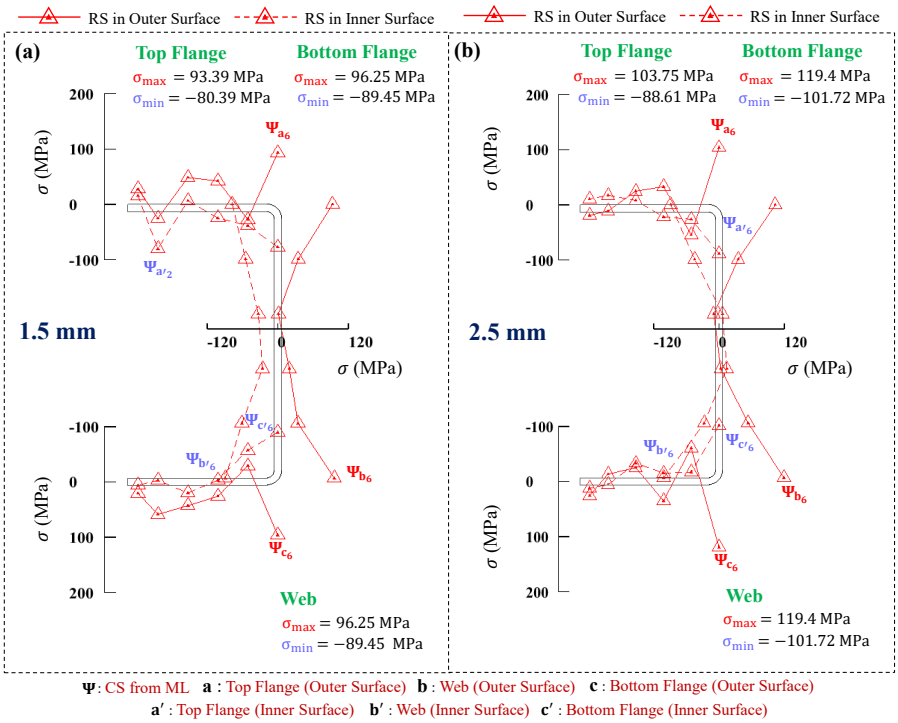


Figure 8: XGBoost-predicted residual stress distributions in PBC sections: (a) 1.5 mm thick sections; (b) 2.5 mm thick sections

$$\varepsilon_{\text{true}}^{\text{pl}} = \ln(1+\varepsilon) - \frac{\sigma_{\text{true}}}{E} \tag{2}$$

where $E$ = Young's modulus, and $\sigma$ and $\varepsilon$ are measured engineering stress and strain values.

The numerical procedure consisted of two stages. First, linear elastic buckling analyses were conducted on perfect columns to extract the lowest global, local, and torsional eigenmodes. These modes were appropriately scaled to define initial geometric imperfections following established expressions (Selvaraj and Madhavan 2020), as shown in Fig. 9(a-d). Second, ML-predicted RS were imposed on flat and corner regions of the section using predefined fields, together with corresponding plastic strain distributions. The engineering stress–strain data were converted to true stress–strain relationships to ensure accurate material representation.

Columns of varying lengths were analyzed to investigate the interaction between RS and buckling behavior.The FE-predicted ultimate strengths ($P_{\text{FEA}}$) were compared with nominal strengths calculated using the Direct Strength Method (DSM) in accordance with the North American Specification for the Design of Cold-Formed Steel Structural Members published by the American Iron and Steel Institute (AISI) Iron and (AISI), as given in Eq.3. DSM predictions generally showed close agreement with FE results across all lengths. Stub columns failed predominantly by local buckling, while longer columns exhibited combined local–flexural buckling, consistent with DSM classifications, as illustrated in Fig. 9(e-g).

$$P_{n,\text{DSM}} = \min(P_{ne}, P_{nl}, P_{nd}) \tag{3}$$

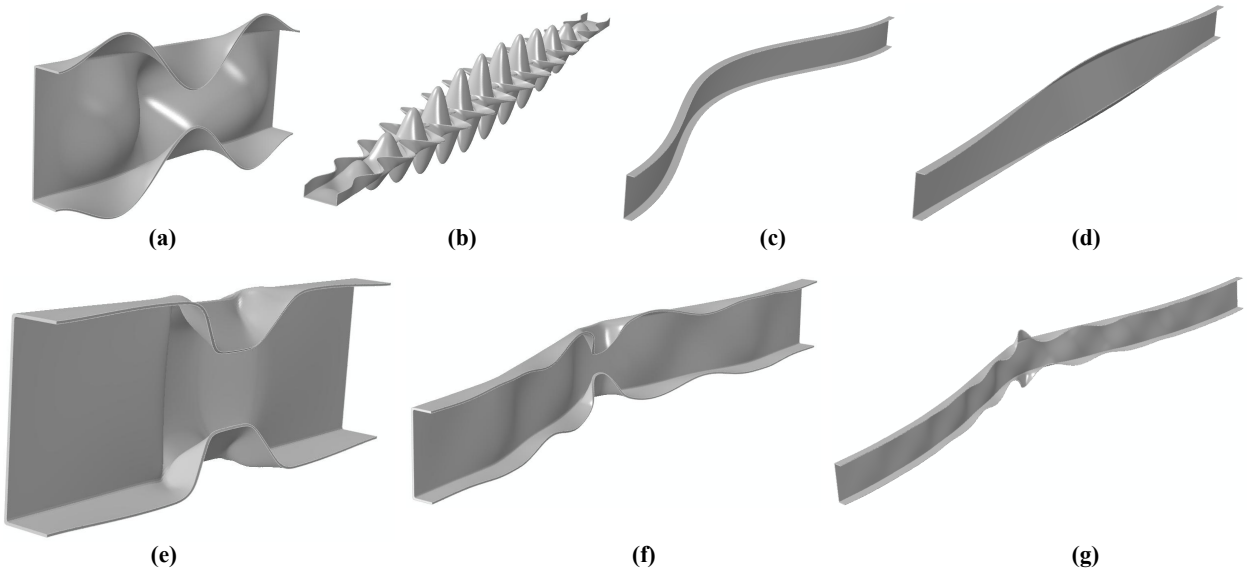


Figure 9: Buckling modes and deformed shapes of CFS columns with 1.5 mm and 2.5 mm thickness: (a) local buckling in short columns; (b) local buckling in long columns; (c) global buckling modes; (d) distortional/torsional (twist) buckling modes; (e–g) failure modes of columns with varying lengths

Residual stresses were found to have a length-dependent influence on column strength. For short columns, RS caused only minor strength reductions (approximately 3–4%). In contrast, long columns experienced more pronounced reductions, reaching about 17% for 1.5 mm sections and 10% for 2.5 mm sections. This trend reflects the dominance of detrimental RS effects over strain-hardening benefits in slender members, particularly where buckling governs failure. The magnitude of strength reduction observed for long columns aligns well with previously reported results for cold-formed carbon steel channels (Quach et al. 2010). Overall, the numerical results confirm that ML-predicted RS can be reliably integrated into FE models and that DSM provides a reasonable and generally conservative estimate of column strength. Residual stresses have a limited effect on short columns but significantly influence the strength and failure mode of slender press-braked CFS members.

### *3.6 Effect of strain hardening at corners*

RS reduce the global buckling resistance of press-braked channel sections, whereas strain hardening at corners (SHC) provides a beneficial counteracting effect by enhancing local material strength (Ellobody and Young 2005). During press braking, sequential bending induces plastic strains at corner regions, resulting in increased corner yield strength ($f_{y,c}$) compared to flat portions (Karren 1967 ; Afshan et al. 2013). The combined presence of SHC and RS influences the overall structural response of cold-formed steel members (Quach et al. 2010).

In this study, SHC was explicitly incorporated together with machine-learning-predicted RS in the finite element (FE) models to quantify its ability to mitigate RS-induced strength reductions. The enhanced corner yield strength was estimated using the model proposed by Rossi et al. Rossi et al. (2013), which has been shown to be broadly applicable to cold-formed steel sections (Gardner and

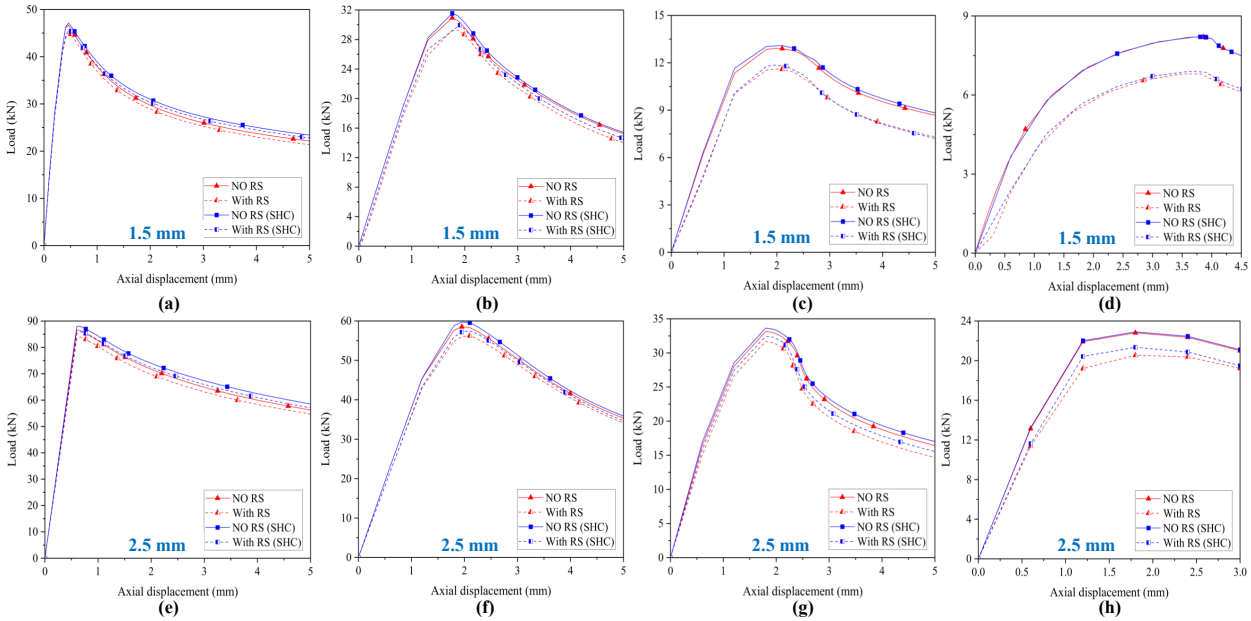


Figure 10: FEA Load–axial displacement curves for CFS columns with different lengths and thicknesses: (a–d) 1.5 mm thick columns and (e–h) 2.5 mm thick columns. Column lengths are (a, e) 350 mm, (b, f) 1000 mm, (c, g) 350 mm, and (d, h) 350 mm

Yun 2018). The corner yield strength is expressed as:

$$f_{y,c} = p(\varepsilon_{c,\mathrm{av}} + \varepsilon_{0.2})^q \leq f_u, \tag{4}$$

where the average corner plastic strain is given by

$$\varepsilon_{c,\mathrm{av}} = \frac{t}{2(2r_i + t)}. \tag{5}$$

Plastic strains at the corners were determined using the revised Ramberg–Osgood formulation for cold-formed steel (Ramberg and Osgood 1943 ; Gardner and Yun 2018), and the corresponding true stress–strain relationships were incorporated into the FE models. Based on this approach, the enhanced corner yield strengths were obtained as 352.4 MPa and 368.3 MPa for the 1.5 mm and 2.5 mm sections, respectively. The numerical results indicate that accounting for SHC reduces the detrimental influence of RS on column strength. Compared with FE models considering RS alone, the inclusion of SHC led to an increase in axial capacity of approximately 1–2% for the 1.5 mm sections and 2–4% for the 2.5 mm sections. The maximum strength enhancement was 2.3% for the 1.5 mm columns and 3.9% for the 2.5 mm columns. For long columns governed by combined local–flexural buckling, the strength reduction due to RS decreased from 17.0% to 16.0% for the 1.5 mm sections and from 9.9% to 6.8% for the 2.5 mm sections when SHC was considered, as summarized in Table 2 and Fig. 10. These results demonstrate that SHC partially compensates for RS-induced strength loss, with a more pronounced benefit observed in thicker sections. Overall, the findings confirm that incorporating SHC is essential for realistic strength assessment of press-braked CFS columns and improves agreement with Direct Strength Method predictions and observed failure modes.

Table 2: Comparison of FE and DSM column strengths considering corner strain hardening in CFS columns

| End Condition | L (mm) | FEA (strain hardening at corners) | | | Strength enhancement (Diff. between RS and RS with strain hardening at corners) (%) | DSM ($P_{DSM}$) (in kN) | $\frac{P_{FEA}}{P_{DSM}}$ |
|---|---|---|---|---|---|---|---|
| | | Presence of RS | $P_{FEA}$ (in kN) | Decrease in Load (%) | | | |
| **(For 1.5 mm)** | | | | | (compare the $P_{FEA}$ of table 6) | | |
| | 350 | No RS | 47.13 | | | | |
| | | With RS | 45.48 | 3.50 | 1.21 | 47.63 | 0.95 |
| | 1000 | No RS | 31.54 | | | | |
| | | With RS | 29.95 | 5.02 | 2.33 | 26.15 | 1.14 |
| Fixed-ended | 2000 | No RS | 13.09 | | | | |
| | | With RS | 11.85 | 9.45 | 2.17 | 10.11 | 1.17 |
| | 3000 | No RS | 8.20 | | | | |
| | | With RS | 6.89 | **16.02** | 1.25 | 6.82 | 1.00 |
| | | | | | Mean | | **1.06** |
| **(For 2.5 mm)** | | | | | | | |
| | 350 | No RS | 88.03 | | | | |
| | | With RS | 85.85 | 2.48 | 2.42 | 80.55 | 1.06 |
| | 1000 | No RS | 59.74 | | | | |
| | | With RS | 57.46 | 3.81 | 2.19 | 49.64 | 1.15 |
| Fixed-ended | 2000 | No RS | 33.64 | | | | |
| | | With RS | 32.45 | 3.53 | 2.52 | 28.37 | 1.14 |
| | 3000 | No RS | 22.90 | | | | |
| | | With RS | 21.34 | **6.81** | 3.91 | 22.77 | 0.93 |
| | | | | | Mean | | **1.07** |

∗ ”No RS” considers only geometric imperfections.

∗ ”With RS” considers both geometric imperfections and RS.

∗ ”L” represents Local buckling and ”F” represents Flexural buckling.

## 4. Conclusions

This study experimentally quantified residual stresses in press-braked cold-formed steel unlipped channel sections of two thicknesses using X-ray diffraction. The measured RS, characterized by significant spatial variability, were subsequently modeled using machine learning to develop predictive RS distributions. A finite element framework implemented in ABAQUS was then employed to evaluate the influence of ML-predicted RS on the axial strength of press-braked unlipped channel columns. The numerical results demonstrate that RS-induced reductions in axial capacity are more pronounced in longer columns, in close agreement with trends reported in the literature Quach et al. (2010).

This study investigated residual stress behavior in press-braked cold-formed steel unlipped channel sections of 1.5 mm and 2.5 mm thickness using X-ray diffraction. The measured RS, characterized by significant spatial variability, were subsequently modeled using machine learning (ML) to develop predictive RS distributions. A finite element framework implemented in ABAQUS was then employed to evaluate the influence of ML-predicted RS on the axial strength of press-braked unlipped channel columns. The numerical results demonstrate that RS-induced reductions in axial capacity are more pronounced in longer columns, in close agreement with trends reported in the literature (Quach et al. 2010). Based on the results, the following conclusions are drawn:

- XRD measurements show significant RS variability across the cross-section for both thicknesses, with the highest tensile residual stress (TRS) consistently occurring at outer bent locations and compressive residual stress (CRS) at inner surfaces. Peak RS reached approximately 60% (TRS) and 48% (CRS) of $f_y$ for 1.5 mm sections and 65% (TRS) and 41% (CRS) for 2.5 mm sections.

- Flat flange and web regions exhibit highly scattered RS with no distinct trend. RS variation is more pronounced in flanges than in webs. The 1.5 mm sections show greater inner–outer RS variation in the web, whereas the 2.5 mm sections exhibit comparable variation on both web surfaces.

- The ML-based XGBoost model accurately predicts RS distributions for both thicknesses, capturing self-equilibrating stress patterns and correctly identifying peak RS at bent locations. The model demonstrates high predictive accuracy without overfitting and reliably reflects experimentally observed thickness effects.

- Finite element analysis incorporating ML-predicted RS successfully captures the axial behavior of press-braked columns. Stub columns fail by local buckling, while longer columns exhibit local–flexural interaction, consistent with Direct Strength Method (DSM) predictions.

- Residual stresses reduce axial strength more significantly in longer columns, with reductions of approximately 17% for 1.5 mm and 9–10% for 2.5 mm sections, compared to 3–4% in short columns. These trends closely align with existing literature (Quach et al. 2010).

- Strain hardening at corners (SHC) partially offsets the detrimental effects of RS, enhancing column strength by approximately 1–2% for 1.5 mm and 2–4% for 2.5 mm sections. The beneficial influence of SHC is more pronounced in thicker sections, reducing RS-induced strength loss in long columns.

## Acknowledgments

The authors gratefully acknowledge the Anusandhan National Research Foundation (ANRF) (CRG/2022/000026), Department of Science and Technology, Government of India, for funding this research work.

## References

Afshan, S., Rossi, B., and Gardner, L. (2013). "Strength enhancements in cold-formed structural sections—Part I: Material testing". *Journal of Constructional Steel Research*, 83:177–188.

Batista, E. M. and Rodrigues, F. C. (1992). "Residual stresses measurements on cold-formed profiles". *Experimental Techniques*, 16:25–29.

Belassel, M., Pineault, J., and Brauss, M. (2004). "Application of X-ray diffraction for residual stress determination in mechanical components". *Proceedings of the ASME International Mechanical Engineering Congress and Exposition*, pages 1–8.

Bragg, W. L. (1912). "The diffraction of short electromagnetic waves by a crystal". *Proceedings of the Cambridge Philosophical Society*, 43:191–203.

Celard, N. J. C., Pathiraj, B., Nikbin, K., and Webster, G. A. (2000). "A comparison of residual stress measurements in steels using the X-ray and neutron diffraction techniques". *Materials Science Forum*, 347–349:316–321.

Cooper, A. S. (1962). "Precise lattice constants of germanium, aluminum, gallium arsenide, uranium, sulphur, quartz and sapphire". *Acta Crystallographica*, 15(6):578–582.

Duan, N. Q., Ren, J., and Pang, R. Q. (2012). "The experimental study of diffraction angle of aluminum alloy 3003". *Advanced Materials Research*, 625:291–296.

Ellobody, E. and Young, B. (2005). "Behavior of cold-formed steel plain angle columns". *Journal of Structural Engineering*, 131(3):457–466.

Gardner, L. and Yun, X. (2018). "Description of stress–strain curves for cold-formed steels". *Construction and Building Materials*, 189:527–538.

Genzel, C., Denks, I. A., and Klaus, M. (2012). "Residual stress analysis by X-ray diffraction methods". In *Residual Stress Analysis*, pages 127–146.

Hibbitt, Karlsson and Sorensen, Inc. (2002). *"ABAQUS standard user's manual"*. USA, version 6.3 edition.

Iron, A. and (AISI), S. I. (2016). *"North American Specification for the Design of Cold-Formed Steel Structural Members"*. American Iron and Steel Institute, Washington, D.C.

Jandera, M. and Machacek, J. (2007). "Residual stresses and strength of hollow stainless steel sections". In *Proceedings of the 9th International Conference on Modern Building Materials, Structures and Techniques*, pages 262–263.

Karren, K. (1967). "Corner properties of cold-formed shapes". *Journal of the Structural Division, ASCE*, 93(1):401–433.

Lee, G. C. and Ketter, R. L. (1958). "The influence of residual stress on the strength of members of high-strength steel". Technical report, Fritz Laboratory, Lehigh University.

Ma, J.-L., Chan, T.-M., and Young, B. (2015). "Material properties and residual stresses of cold-formed high-strength steel hollow sections". *Journal of Constructional Steel Research*, 109:152–165.

PROTO Manufacturing (2016). *"PROTO residual stress analyzer hardware manual"*. Windsor, Ontario, Canada, ixrd portable systems edition.

Quach, W. M., Teng, J. G., and Chung, K. F. (2009a). "Residual stresses in press-braked stainless steel sections, I: Coiling and uncoiling of sheets". *Journal of Constructional Steel Research*, 65(8):1803–1815.

Quach, W. M., Teng, J. G., and Chung, K. F. (2009b). "Residual stresses in press-braked stainless steel sections, II: Press-braking operations". *Journal of Constructional Steel Research*, 65(8):1816–1826.

Quach, W. M., Teng, J. G., and Chung, K. F. (2010). "Effect of the manufacturing process on the behaviour of press-braked thin-walled steel columns". *Engineering Structures*, 32(11):3501–3515.

Ramberg, W. and Osgood, W. R. (1943). "Description of stress–strain curves by three parameters". Technical Report Technical Note No. 902, National Advisory Committee for Aeronautics.

Rossi, B., Afshan, S., and Gardner, L. (2013). "Strength enhancements in cold-formed structural sections—Part II: Predictive models". *Journal of Constructional Steel Research*, 83:189–196.

Selvaraj, S. and Madhavan, M. (2020). "Geometric imperfection measurements and validations on cold-formed steel channels using 3D noncontact laser scanner". *Journal of Structural Engineering*, 144(3):ce13p1009.

Somodi, B. and Kövesdi, B. (2017). "Residual stress measurements on cold-formed HSS hollow section columns". *Journal of Constructional Steel Research*, 128:706–720.

Suzuki, K. and Shobu, T. (2010). "Residual microstress of austenitic stainless steel due to tensile deformation". *Materials Science Forum*, 652:7–12.

Wang, F., Yang, J., Azim, I., Bai, L., and Ma, Y. (2020). "Experimental and numerical evaluations of the distribution and effect of roll-forming residual stress on CFS sigma beams". *Journal of Constructional Steel Research*, 167:105978.

Weng, C. C. and Pekoz, T. (1990). "Compression tests of cold-formed steel columns". *Journal of Structural Engineering*, 116(12):1230–1246.

Young, B. and Lui, W. M. (2005). "Behaviour of cold-formed high strength stainless steel sections". *Journal of Structural Engineering*, 131(11):1738–1745.